Macromolecules

Article

Cite This: Macromolecules 2018, 51, 5336−5345

Conformational and Dynamic Properties of Poly(ethylene oxide) in $BMIM^+BF_4^-$: A Microsecond Computer Simulation Study Using ab Initio Force Fields

Chang Yun Son, Jesse G. McDaniel, Qiang Cui, and Arun Yethiraj*

Department of Chemistry and Theoretical Chemistry Institute, University of Wisconsin—Madison, 1101 University Avenue, Madison, Wisconsin 53706, United States

Supporting Information

ABSTRACT: The behavior of polymers in complex solvents is interesting from a fundamental perspective and of practical importance from the standpoint of polymer processing. There has been recent interest in the conformational and dynamic properties of polymer in room temperature ionic liquids, with conflicting predictions from computations using models with different resolutions and conflicting results of experiments from different groups. In this work, we develop a first-principles, nonpolarizable united atom (UA) force field for a mixture of poly(ethylene oxide) (PEO) in the ionic liquid $BMIM^+BF_4^-$. The UA force field is benchmarked against ab initio calculations, and the PEO atomic charges are parametrized to implicitly capture the polarization contribution to the solvation energy of a single PEO molecule in $BMIM^+BF_4^-$. The UA model allows one to perform multi-microsecond molecular dynamics simulations. This is necessary because the conformational relaxation correlation times are of the order of 100 ns. The simulations predict that the radius of gyration, R_g, scales with molecular weight, $R_g \sim M_w^{\nu}$ with $\nu \approx 0.56$ in the temperature range 300−600 K, consistent with experiment, seemingly in between a self-avoiding walk and an ideal chain. An examination of the snapshots of the polymer demonstrates, however, that the polymer conformations are composed of ringlike and linear segments, with ringlike parts of the chain wrapped around cations of the ionic liquid. The slow dynamics arises from the barrier to unwrapping the ringlike segments of the polymer. The mean-square displacement shows three regimes which we interpret as confinement, Zimm, and diffusive. The simulations emphasize the importance of accurate force fields and microsecond simulations in obtaining reliable results for polymers and elucidate important correlation effects for polymers in strongly interacting solvents.

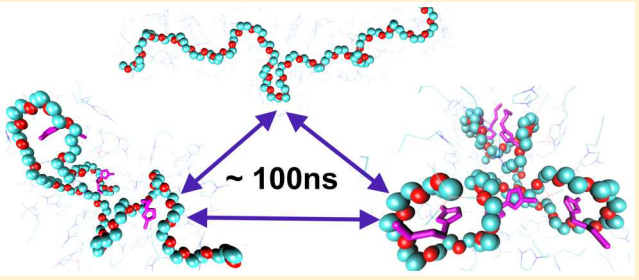

1. INTRODUCTION

Room temperature ionic liquids (ILs) are of considerable scientific and practical importance. They have many potential applications, e.g., as electrolytes in fuel cells, capacitors, and batteries.[1,2] In many applications polymeric scaffolds are envisaged as a means of providing mechanical strength to the working liquid,[3] and the properties of polymer/IL mixtures are therefore of considerable interest.[4] There have been many studies, for example, of the phase behavior of poly(ethylene oxide) (PEO) mixed with imidazolium-based ionic liquids.[5−11] These mixtures exhibit complex behavior for which a detailed microscopic understanding is lacking.

The present work is concerned with the properties of single PEO chains in ionic liquids, which has been a topic of recent discussion. In particular, there has been some controversy regarding the scaling of polymer size with molecular weight in ionic liquids, at room temperature. From a polymer physics standpoint, since PEO and IL are mixed at room temperature, one expects that the IL is a good solvent, and therefore the radius of gyration, R_g, should scale with the degree of polymerization, N, as $R_g \sim N^{\nu}$, with $\nu \approx 3/5$. As the temperature is increased, the system phase separates; i.e., the solvent quality decreases, and hence ν is expected to decrease. Triolo et al.[12] studied the conformational properties of PEO in 1-butyl-3-methylimidazolium tetrafluoroborate ($BMIM^+BF_4^-$) using small-angle neutron scattering (SANS) at 298 K. They did not access the dilute solution regime, but in semidilute solutions they found that R_g scaled with concentration, c, as $R_g \sim c^{0.25}$ which corresponds to $\nu = 1$, i.e., rodlike behavior. These analyses and results have been questioned in recent SANS experiments by Kharel and Lodge,[13] who performed SANS experiments at a number of concentrations and extrapolated to zero concentration in order to extract the real, as opposed to apparent, R_g. At 353 K they obtained $\nu = 0.55 \pm 0.02$, consistent with moderately good solvent behavior. A rheological study by Liu et al.[7] shows that $BMIM^+BF_4^-$ behaves as a theta or poor solvent ($\nu \approx 0.48$) for PEO at 353 K. Note that PEO crystallizes in $BMIM^+BF_4^-$ at 338 K,[7,13]

Received: May 10, 2018
Revised: June 22, 2018
Published: July 11, 2018

DOI: 10.1021/acs.macromol.8b01002
Macromolecules 2018, 51, 5336−5345

which complicates experiments at finite concentrations but is not expected to impact the infinite dilution solution behavior.

Computer simulations and integral equation theory studies present a confusing picture. Mondal et al.[14] presented atomistic simulations (utilizing the atomistic OPLS force field) of PEO in $BMIM^+BF_4^-$. There were problems with equilibration at room temperature, and so they employed replica exchange simulations with 64 replicas at different temperatures. They found that $R_g \sim N^{0.9}$ at room temperature, although they noted that the chain lengths they studied ($N \leq 40$) might not have been in the true scaling regime. Later computational work by Choi et al.[15] utilized a coarse-grained model of PEO and $BMIM^+BF_4^-$ and found that the chains were collapsed at 300 and 400 K, in both simulations and self-consistent integral equation theory.

McDaniel et al.[16] recently developed a fully polarizable, atomistic force field based on symmetry adapted perturbation theory (SAPT) for PEO/$BMIM^+BF_4^-$ denoted SAPT-AA. Both OPLS-AA and SAPT-AA force field predicted ideal chain behavior of PEO in $BMIM^+BF_4^-$ at elevated temperatures of 400−600 K. However, the computational demands of these force fields precluded simulations at room temperature.

Molecular simulations of PEO in ILs are challenging because of the sensitivity to interaction potentials and the long simulation time scales. The viscosity of $BMIM^+BF_4^-$ is 100 cP at 300 K compared to ∼10 cP at 350 K.[17] Explicitly polarizable force fields have been developed[16] and show that polarization makes important contributions to both the energetics of the mixture and the relaxation dynamics of the solvent. They are, however, computationally intensive for long chains. Existing nonpolarizable force fields predict IL solvent dynamics that are too slow by an order of magnitude,[18] further worsening sampling problems. Alternative nonpolarizable, "scaled charge" force fields may improve the description of solvent dynamics but fail to capture the cohesive energy of IL/polymer mixtures and thus predict qualitatively incorrect phase behavior, e.g., for PEO/$BMIM^+BF_4^-$ mixtures.[11,19]

In this work, we develop a computationally efficient, first-principles based nonpolarizable united atom (UA) force field for PEO and $BMIM^+BF_4^-$ and study the properties of a single PEO chain in $BMIM^+BF_4^-$ at a range of temperatures, including room temperature. (We employ the nomenclature "PEO*n*" to denote the polymer chain length defined as $CH_3-(O-CH_2-CH_2)_n-O-CH_3$.) The force field parametrization for PEO follows recently developed methodology for generating united atom force fields based on SAPT, which was previously validated for neat $BMIM^+BF_4^-$.[19] Notably, the optimized force field accurately reproduces the cohesive energy of the neat IL, neat PEO oligomers, and the PEO/$BMIM^+BF_4^-$ mixture, indicating a reliable description of the phase behavior. Simulations are performed for single chain PEO in $BMIM^+BF_4^-$ for five different polymer lengths at 300, 400, and 600 K. The $BMIM^+BF_4^-$ behaves as a moderately good solvent for PEO at all the temperatures, consistent with the SANS experiments by Kharel and Lodge.[13] Notably, the room temperature scaling predictions require multi-microseconds simulation times for statistically converged results, which are accessible only with the UA model developed in this work. We find that simultaneous coordination of ions by multiple monomer units of the polymer is a key temperature-dependent specific interaction that may partially account for the entropically driven LCST phase behavior. We find that both computational efficiency and an accurate description of the mixture energetics are required for reliably predicting the properties of polymer/ionic liquid mixtures.

2. SIMULATION METHODS

All molecular dynamics (MD) simulations are performed using the GROMACS version 4.6.5[20] software. The nonbonded van der Waals interactions are shifted to zero at 1.4 nm. Long-range electrostatics are calculated with the particle mesh Ewald (PME) method[21,22] with the real-space cutoff distance of 1.4 nm. For all simulations, the Nosé−Hoover[23,24] thermostat is used to constrain the system temperature. NPT equilibration steps utilize the Berendsen[25] barostat, and the NPT production runs for the density calculations utilize the Parrinello−Rahman[26] barostat. We use 4 fs of time step for all simulations except for the benchmark simulation with polarizable SAPT-AA force field, where 2 fs time step is used. For simulations of neat PEO, five systems are prepared with 350, 250, 200, 200, and 200 molecules of PEO1, PEO2, PEO3, PEO4, and PEO5. The energy of each system is minimized, and the system is then equilibrated for 2 ns at 300 K and 1 bar. Average properties are obtained from 5 ns NPT simulations. The PEO1 system is further simulated for 20 ns in the NVT ensemble at 300 K to characterize the dihedral angle distribution.

Simulations of PEO in $BMIM^+BF_4^-$ are performed for four chain lengths, n = 9, 18, 27, and 40, and for three different temperatures: 300, 400, and 600 K. A single chain of PEO is solvated in $BMIM^+BF_4^-$ with 250, 260, 650, and 1000 ion pairs for n = 9, 18, 27, and 40, respectively. Additionally, we conduct simulations for a system of a single PEO60 chain solvated in ∼3200 ion pairs at 600 K. Two sets of 10 ns equilibration, first in NPT ensemble at 1 bar and then in NVT ensemble, are performed for all the systems. To ensure proper convergence in the conformational properties of PEO, the production NVT simulations are continued for at least a microsecond; PEO9 at 300 and 400 K are simulated for 6 μs, PEO18 at 300 and 400 K as well as PEO27 at 400 K are simulated for 5 μs, and all chains at 600 K are simulated for 1 μs. For PEO27 at 300 K and PEO40 at 300 and 400 K, three sets of initial conformations of the PEO are constructed, namely a random, a collapsed, and an extended conformation, and then simulated for 3−5 μs. The combined simulation times are 12 μs for PEO27 at 300 K, 9 μs for PEO40 at 400 K, and 15 μs for PEO40 at 300 K.

We calculate several conformational and dynamic properties of the polymer. The radius of gyration (R_g) of the polymer is defined as

$$R_g = \left(\frac{\sum_i m_i (\mathbf{r}_i - \mathbf{r}_{com})^2}{\sum_i m_i} \right)^{1/2} \quad (1)$$

where $\mathbf{r}_i$ is the position of site i, m_i is the mass of site i, and $\mathbf{r}_{com}$ is the position of the center-of-mass. The end-to-end distance is defined as

$$R_{ete} = |\mathbf{r}_N - \mathbf{r}_1| \quad (2)$$

where $\mathbf{r}_1$ and $\mathbf{r}_N$ are the positions of the terminal carbon atoms on the polymer chain. The single chain structure factor is defined as

$$S(q) = \frac{1}{\sum_{j=1}^{N} f_j^2} \sum_{i=1}^{N} \sum_{j=1}^{N} f_i f_j \frac{\sin(q r_{ij})}{q r_{ij}} \quad (3)$$

DOI: 10.1021/acs.macromol.8b01002
Macromolecules 2018, 51, 5336−5345

where f_i are the atomic form factors and q is the momentum transfer variable. The radius of gyration autocorrelation function is defined as

$$C_{R_g}(t) = \frac{\langle (R_g(t+\tau) - \langle R_g \rangle)(R_g(\tau) - \langle R_g \rangle) \rangle}{\langle (R_g(\tau) - \langle R_g \rangle)^2 \rangle} \quad (4)$$

We calculate the radial distribution function, $g(r)^{O}_{BMIM^+}$, of the oxygen atoms of the polymer from the center-of-mass of the imidazolium ring of the cation. The coordination number of a cation, $CN^{O}_{BMIM^+}$, is the number of oxygen atoms within a distance r_{cut} of the center-of-mass of the imidazolium ring. We choose $\mathbf{r}_{cut}$ = 5 Å, which is the location of the first minimum in $g(r)^{O}_{BMIM^+}$. The survival probability, $P_{CI}(t)$, of the coordinating ions to the polymer is the probability that an ion is coordinated to an oxygen atom, i.e., ion center-of-mass distance is less than r_{cut}, at time $t + \tau$ given that it was coordinated at time τ to the same oxygen atom, averaged over all τ and all monomers.

3. FORCE FIELD DEVELOPMENT

We develop a united atom (UA) force field for PEO that is consistent with the UA force field for $BMIM^+BF_4^-$ reported previously.[19] We refer to this combined PEO/$BMIM^+BF_4^-$ force field as "SAPT-UA" because the parametrization is based on ab initio DFT-SAPT[27−29] calculations. Two new UA types are developed for PEO (denoted CD and CT for the CH_2 and CH_3 groups, respectively).

DFT-SAPT provides an explicit energy decomposition of intermolecular interaction energies, given by

$$E_{tot} = E_{exch} + E_{elec} + E_{ind} + E_{disp} + E_{dhf} \quad (5)$$

so that the total interaction energy is a sum of exchange-repulsion (E_{exch}), electrostatic (E_{elec}), induction (E_{ind}), dispersion (E_{disp}), and higher-order (E_{dhf}) contributions. We note that second-order exchange terms are grouped with their induction and dispersion energy counterparts, as done previously.[30] The force field is then constructed to reproduce this energy decomposition, and in this regard there are two distinct classes of force field parameters: long-range, asymptotic parameters (dispersion coefficients) are derived from monomer response calculations, and short-range interaction parameters (exponential terms) are fit to residual energies from homodimer DFT-SAPT calculations; further details can be found in previous work.[19,30] A primary difference with previous work is that the present model is nonpolarizable and represents a nonhomogeneous IL/PEO mixture system. While omitting explicit polarization did not affect the cohesive energy of homogeneous neat IL,[19] this is not the case for the mixture system. Thus, in this work, there is no longer a one-to-one correspondence between the force field and SAPT electrostatic and induction energies, but rather the sum of the terms is fit; this necessitates additional parametrization steps, as discussed below.

The SAPT-UA force field development for PEO has three steps: (i) fit all short-range, nonbonded interaction parameters to gas-phase DFT-SAPT calculations for PEO1 and PEO2 dimers; (ii) fit the charge on the PEO to reference simulations of single dimethyl ether (PEO0) in liquid $BMIM^+BF_4^-$ conducted with polarizable, all-atom SAPT-AA model; and (iii) fit the dihedral potential to relaxed ab initio potential energy scans using the parameters from (i) and (ii). The steps are described below.

The short-range, nonbonded interaction parameters are fit to reproduce the DFT-SAPT calculated homomolecular interaction energies of PEO1 and PEO2. Specifically, such parameters for CD and CT are optimized for each of the four SAPT energy components, with these SAPT calculations taken from the work of McDaniel et al.[16] The dispersion parameters for CD and CT are taken from SAPT-UA $BMIM^+$[19] with slight adjustment (Supporting Information). All remaining parameters including those of oxygen atom type are taken from McDaniel et al.[16] Intramolecular bond and angle force field parameters for PEO are adapted from the OPLS force field.[31] We note that dimer configurations for fitting and the resulting force field parameters have been iteratively optimized (2−3 cycles) to convergence utilizing liquid MD simulations.[16]

The SAPT-UA model has only one charge parameter $q_O = 1/2q_{CT} = 1/2q_{CD}$, and this parameter is tuned to reproduce the electrostatic cross-cohesive energy of a dimethyl ether molecule (PEO0) in $BMIM^+BF_4^-$ in SAPT-AA simulations.

We calculate benchmark values for the electrostatic cohesive energy between PEO0 and $BMIM^+BF_4^-$ from simulations of a single PEO0 molecule in 250 $BMIM^+BF_4^-$ ion pairs, interacting via the SAPT-AA model.[16] The cross cohesive energy is obtained by subtracting from the total energy all intramolecular energy and intermolecular energy between IL pairs. The parameter q_O is systematically varied ($0.43e \le q_O \le 0.65e$) to fit the cross cohesive energy at 400 K. For each value of q_O parameter UA simulations are performed, and the electrostatic, van der Waals (vdW), and the total cross-cohesive energies are compared with the quantities from SAPT-AA. As shown in Figure 1, the electrostatic part of the

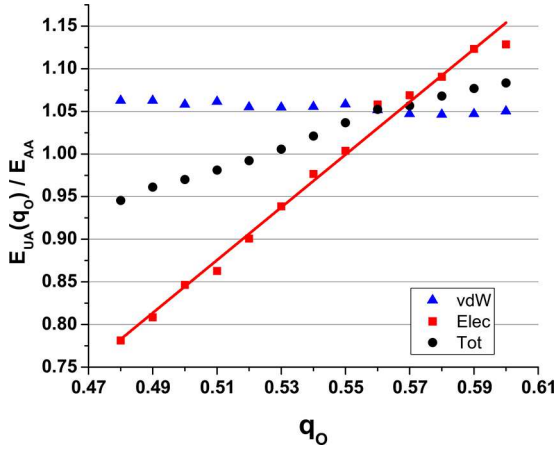

Figure 1. Comparison of relative cross-cohesive energies of SAPT-UA force field to that of SAPT-AA force field as a function of the charge parameter of SAPT-UA force field (q_O) calculated for a dimethyl ether molecule in $BMIM^+BF_4^-$. The total cross-cohesive energies (black circles) are decomposed into van der Waals (blue triangles) and electrostatic (red squares) terms.

cohesive energies shows strong linear correlation to the charge parameter q_O; we find an optimal value of $q_O = 0.55e$, which reproduces the SAPT-AA energetics. Note that we do not compensate for the ~5% error in the vdW energy but only match the electrostatic contribution to the cross-cohesive energy with q_O.

Interestingly, the gas-phase PEO2−dimethylimidazolium ($MMIM^+$) interaction energy calculated with the optimized SAPT-UA model shows remarkable agreement to the SAPT

DOI: 10.1021/acs.macromol.8b01002
Macromolecules 2018, 51, 5336−5345

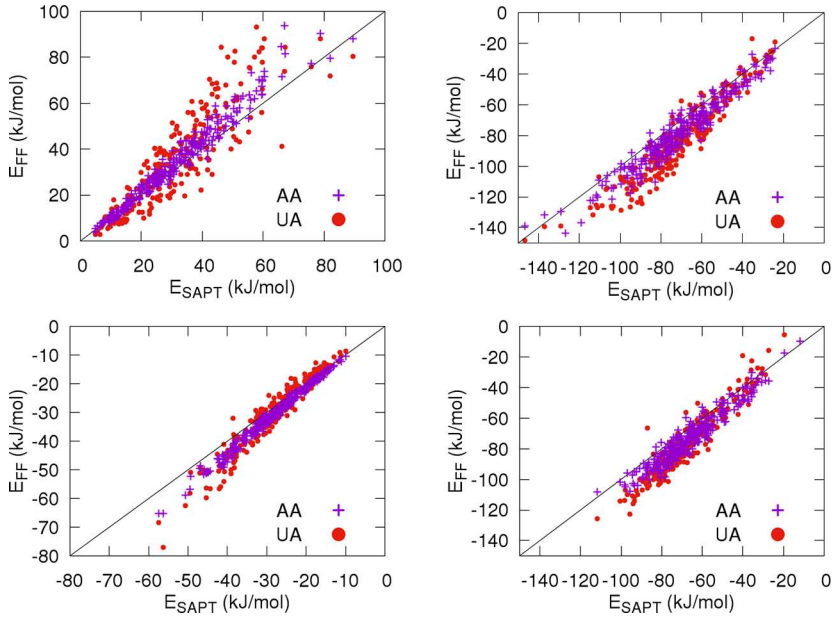

Figure 2. Comparison of intermolecular interaction energies between PEO2 and $MMIM^+$ calculated by SAPT-UA and SAPT-AA force fields (y-axis) to the DFT-SAPT calculated energies (x-axis). From top to bottom, left to right: exchange, electrostatic + induction + dhf, dispersion, and total energy.

interaction energies (Figure 2). This results from a compensation between overestimated electrostatic energy due to higher charge parameter (q_O(UA) = 0.55e vs q_O(AA) = 0.4315e) and the underestimated induction energy due to ignoring the explicit polarization in the nonpolarizable force field (Figure S5). While using the charge parameters of SAPT-AA reproduces the DFT-SAPT electrostatic energies, it underestimates the total gas phase dimer interaction strength (Figure S5). As shown in Figure 1, this compensation between ignored polarization and enhanced electrostatics is necessary to reproduce the cohesive energy between PEO and $BMIM^+BF_4^-$ in the mixture.

We fit the dihedral potentials of the PEO SAPT-UA model to the ab initio relaxed potential energy surface (PES) scan calculated by Anderson and Wilson[32] for PEO1. Note that we exclude the 1−4 intramolecular nonbonded interactions, unlike the original OPLS-AA force field. A comparison of the force field conformational energies to the ab initio PES is shown in Figure 3 for three different PEO1 geometries as a function of the O−C−C−O and C−O−C−C dihedral angles. It is seen that the force field reproduces the ab initio PES for TXT and TTX with high fidelity, accurately capturing the relative energies of the local minima and torsional barriers. The UA-TGX dihedral scan deviates from AI-TGX PES and has narrower distribution near the angle of 0 and 300°. We attribute this to the large exchange-repulsion parameter of the terminal CH_3 group coming from the united atom level description. The methyl group hydrogen rotation relaxes the dihedral surface. In the TGX and TTX scans, the methyl group on the end of PEO1 interacts (sterically) with the oxygen when the dihedral is close to 0 and 360°. The methyl group will rotate to relax this interaction, but this is not present in the UA force field and is only captured if the dihedral potential is explicitly fit (as is the case with TXT). The UA carbon is thus too repulsive in a sense for this conformation, and so that is why the force field has an artificial repulsive wall from 0−60 and 300−360 for this dihedral potential. We anticipate this

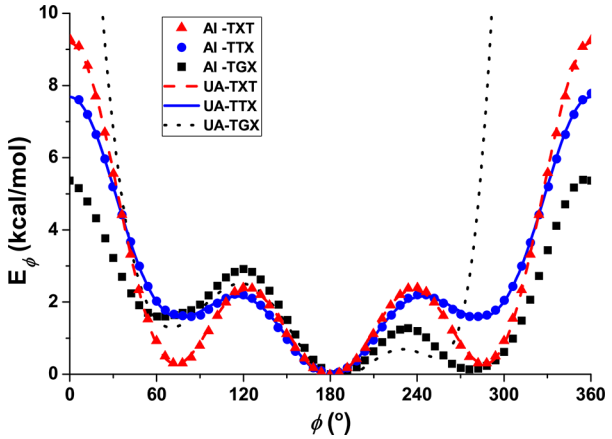

Figure 3. Optimized force field fits for three dihedral angles (ϕ) of PEO1 in SAPT-UA model (UA) compared to the ab initio (AI) calculations of relaxed potential energy surface scans taken from ref 32. The first C−O−C−C dihedral angles is fixed in trans (T) orientation, and one of the central O−C−C−O and the last C−O−C−C dihedral angle is varied (X) while the other is fixed in either trans (T) or gauche (G) orientation.

discrepancy to be only minor significance for long polymer chains, and the dihedral potentials used here produce physical dihedral angle distributions at equilibrium even for short oligomers.

Interestingly, we find that the dihedral potential has a significant influence on the system density, as employing the original OPLS-AA dihedrals instead of the newly optimized dihedral potential give density differences of ∼2% for neat PEO1. The dihedral distribution of neat PEO1 at 300 K sampled with the final SAPT-UA force field is shown in Figure 4. As speculated by McDaniel et al.,[16] the peak positions of ϕ_{OCCO} predicted by both the SAPT-AA and OPLS-AA force field are off by ∼15° (Figure 4), as benchmarked to the ab initio parametrized SAPT-UA model. Furthermore, the populations of the gauche orientation of ϕ_{COCC} and of the

DOI: 10.1021/acs.macromol.8b01002
Macromolecules 2018, 51, 5336−5345

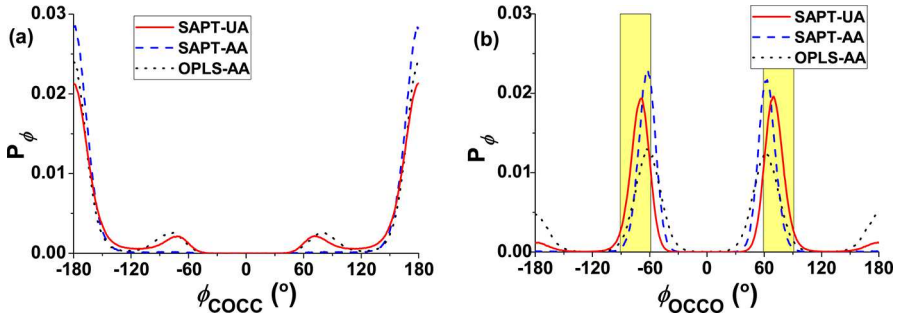

Figure 4. Predicted distributions of dihedral angles (a) C−O−C−C (ϕ_{COCC}) and (b) O−C−C−O (ϕ_{OCCO}) in liquid state neat PEO1 at 300 K in three different force fields. The SAPT-AA and OPLS-AA simulation results are obtained from ref 16. The highlighted area in (b) represents the range of ϕ_{OCCO} that are within a k_BT of the local minima shown in Figure 3.

trans orientation of ϕ_{OCCO} are not sampled by SAPT-AA, which is the reason for the restricted polymer conformations and corresponding underpredicted densities of neat PEO oligomers from previous SAPT-AA simulations.[16] This suggests that the intramolecular dihedral potential for a flexible polymer needs to be consistently parametrized with the nonbonded interaction potential, which was not the case in the SAPT-AA force field where the OPLS dihedral potential was used with the scaled SAPT-AA nonbonded interaction for 1−4 atom pairs.

4. RESULTS AND DISCUSSION

4.1. Conformational Relaxation Time. The conformational relaxation times of the polymer in $BMIM^+BF_4^-$ are sufficiently long that sampling conformational space in simulations is challenging and requires simulations of several microseconds long. Figure 5 depicts the radius of gyration, R_g, as a function of time in three independent simulations starting from different initial configurations, i.e., randomly generated chain (set 1), extended chain (set 2), and collapsed chain (set 3). The "memory" of the initial condition is lost within a few hundred nanoseconds, but there are large variations in chain size as a function of time. As a consequence simulations of several microseconds in duration are required to obtain statistically significant results, which are orders of magnitude longer than usually reported in the literature. Figure 5 also argues that the simulations of this work adequately sample conformational space because widely differing initial configurations give similar values for $\langle R_g^2 \rangle^{1/2}$.

The large conformational relaxation times can be quantified by considering the normalized time correlation functions of R_g (eq 4). Figure 6 depicts $C_{R_g}(t)$ for PEO40 in $BMIM^+BF_4^-$ at

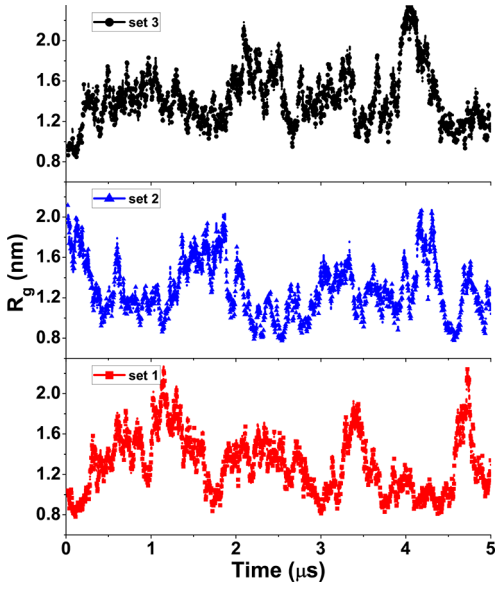

Figure 5. Radius of gyration of single PEO40 chain in $BMIM^+BF_4^-$ at 300 K from three independent simulations initiated with different initial configurations: an intermediate random conformation (set 1), an extended chain (set 2), and a collapsed chain (set 3).

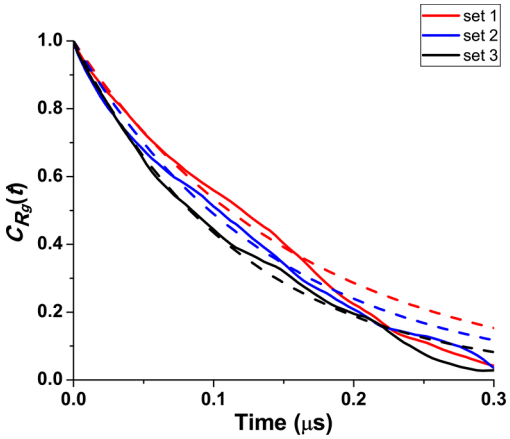

Figure 6. Time correlation function ($C_{R_g}(t)$) of R_g for PEO40 at 300 K. The three different colors indicate the different sets described in Figure 5. The dashed lines are an exponential fit to $C_{R_g}(t) = \exp(-t/\tau)$, with values of τ = 160, 140, and 120 ns for set 1, 2, and 3, respectively.

300 K. By fitting the function to an exponential at short times (dashed lines), we estimate correlation times of 120, 140, and 160 ns for the three sets.

4.2. Conformational Properties. The Flory scaling exponent, ν, observed in the simulations is in between that of a self-avoiding walk and ideal chain. Figures 7a and 7b depict the root-mean-square radius of gyration and end-to-end distance as a function of molecular weight at three different temperatures. Within the (admittedly large) statistical uncertainties, the chain size is independent of temperature. For the two cases, we fit exponents of ν = 0.56 and 0.51, respectively, which is consistent with recent measurements of Kharel and Lodge[13] and with the ideal chain scaling seen in simulations of the fully polarizable model at 600 K.[16] This scaling is not consistent with previous simulations of Mondal

DOI: 10.1021/acs.macromol.8b01002
Macromolecules 2018, 51, 5336−5345

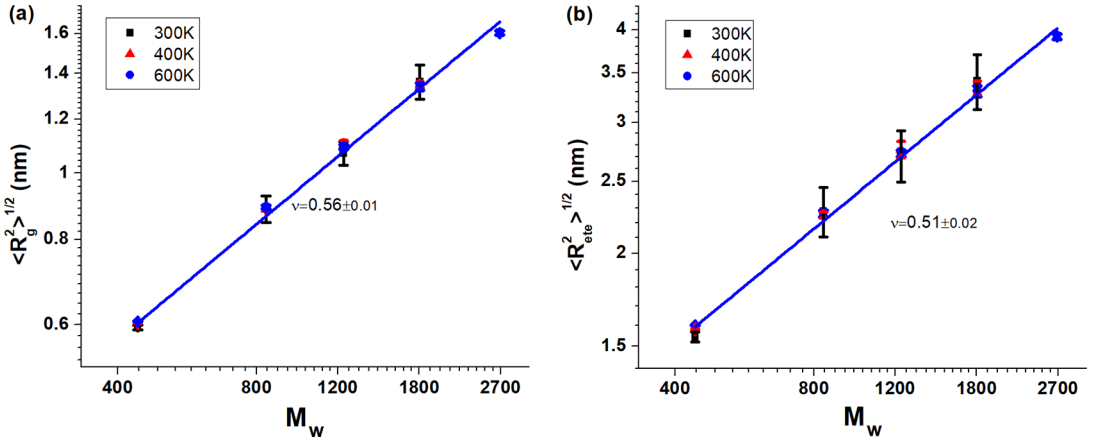

Figure 7. Variation of (a) root-mean-square radius of gyration ($\langle R_g^2 \rangle^{1/2}$) and (b) root-mean-square end-to-end distance ($\langle R_{ete}^2 \rangle^{1/2}$).

et al.,[14] which we attribute to the shorter simulation times studied by those authors. A closer examination of the trends in Figure 7 suggests it is possible that the scaling exponent decreases with increasing temperature, from $\nu \approx 0.57$ at 300 K to $\nu \approx 0.5$ at 600 K, but large statistical uncertainties preclude a definitive statement.

The single chain structure factor provides a more complex picture of polymer conformations than the scaling behavior. Figure 8 depicts $S(q)$ plotted in standard Kratky form. In the intermediate scaling regime, $q^2S(q) \sim q^{2-1/\nu}$, which implies the curve will be flat for an ideal chain, an increasing (decreasing) function of q for a more expanded (compact) chain. At 300 K the Kratky plot shows a dip, suggesting compact structures at the length scale of 1−2 nm, which can be attributed to the "ring" conformation of the polymer wrapping around the cation (see below). As the temperature is increased, the curve flattens out in the intermediate scaling regime which is consistent with ideal scaling.

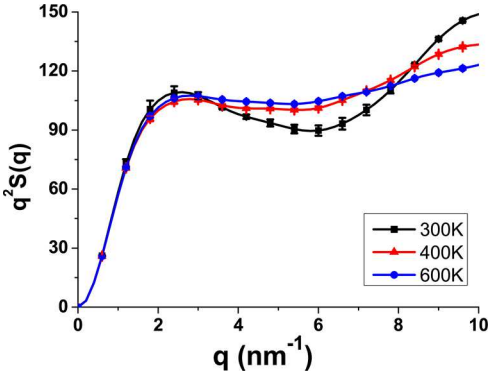

Figure 8. Kratky plot of the single-chain structure factor for PEO27 at three different temperatures.

The probability distribution function of R_g, $P(R_g)$, shows bimodal character, suggesting that the chain occurs in a mixed conformational state. Figure 9 depicts $P(R_g)$ for PEO9 and PEO40. There is a hump in the distribution function at low values of R_g, which is particularly noticeable for PEO9 at 300 K, although it is also present for the higher temperatures and longer chain. In Figure 10, the representative conformations of

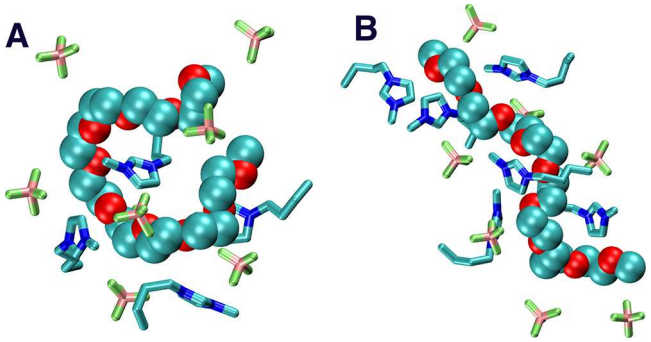

Figure 10. Representative snapshots showing two different conformations of PEO9 corresponding to the peaks in $P(R_g)$ (positions A and B) in Figure 9a. (A) The entire PEO9 chain is wrapped around a single cation. (B) The polymer chain is in a more extended conformation.

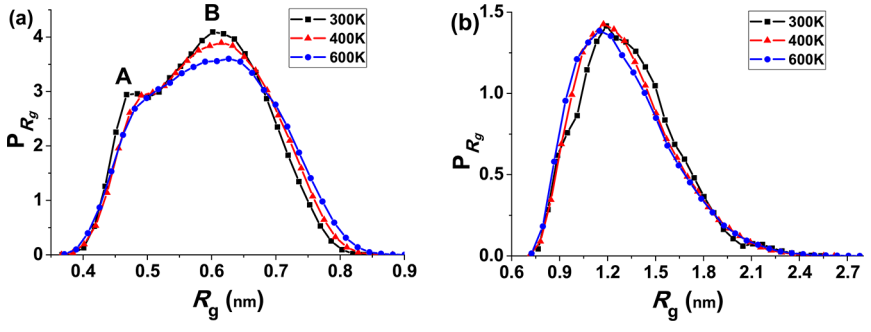

Figure 9. Probability distribution of radius of gyration for (a) PEO9 and (b) PEO40.

DOI: 10.1021/acs.macromol.8b01002
Macromolecules 2018, 51, 5336−5345

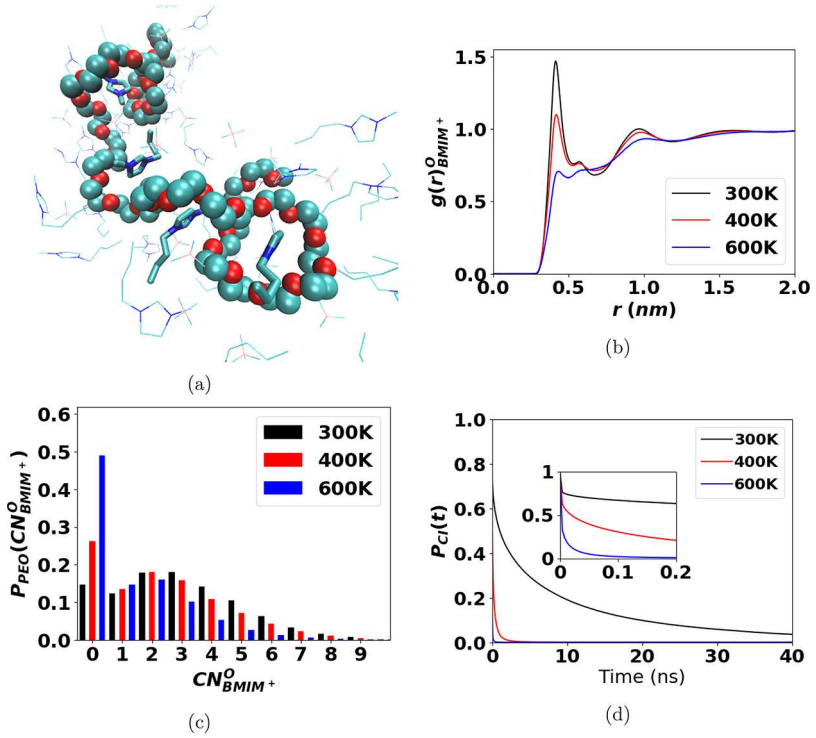

Figure 11. Temperature dependence of the specific PEO/BMIM$^+$ interaction. (a) Typical snapshot of PEO40 at 300 K showing "ring" and "linear" segments. The cations with $CN^{O}_{BMIM^+} \geq 4$ are highlighted. (b) Radial distribution function of the oxygen atoms from the center-of-mass of the imidazolium ring of the cations. (c) Population histogram of PEO monomers that are coordinated to the BMIM$^+$ cations with certain coordination number $CN^{O}_{BMIM^+}$. (d) Survival probability ($P_{CI}(t)$) of the coordinating cations. (inset) Short-time decay of the survival probability showing the fast initial decay.

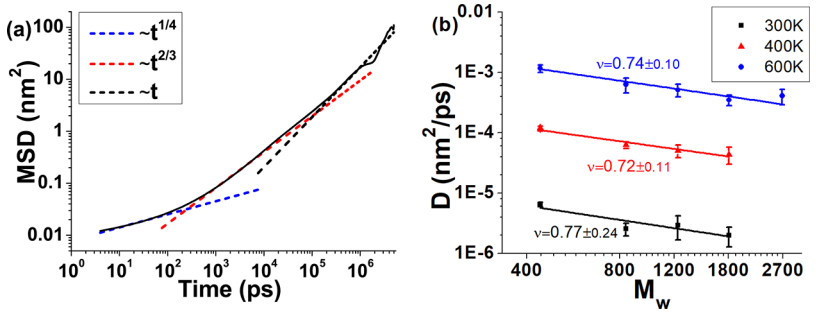

Figure 12. (a) Monomer mean-square displacement (MSD) of PEO40 at 300 K. Dashed lines are a guide to the eye and have slopes corresponding to different regimes. (b) Scaling of the self-diffusion coefficients with M_w with slopes as marked.

the PEO9 corresponding to the two peaks (marked A and B) of the R_g distribution at 300 K are shown, as are nearby ions of the solvent. In both conformations A and B, the multiple oxygen atoms of the polymer are coordinated with the same cation, and the anions are closer to the alkyl carbon atoms of the polymer. However, the nature of the polymer−cation interaction is very different in the two cases, with the polymer wrapping around the cation in conformation A and in a more linear structure in conformation B.

A combination of "ring" and "linear" segments is also found in the longer chains. A typical snapshot of PEO40 is shown in Figure 11a. The number of rings changes during the course of the simulation, ranging from 0 to 5 for PEO40. A cation fully wrapped with the polymer typically has six or more oxygen atoms in direct coordination (within 5 Å distance from the imidazolium center) and has more monomers in proximity. Thus, in PEO9 the entire chain is involved in the formation of a ring, while in longer chains only part of the chain takes on these wrapping conformations. As a consequence, the ring formation is more dramatic in the shorter chains.

The coordination of the PEO to the BMIM$^+$BF$_4^-$ shows a strong temperature dependence. The magnitude of the first peak in the radial distribution function $g(r)^{O}_{BMIM^+}$ (Figure 11b) decreases drastically as the temperature increases, indicating the cations are less coordinated with the polymer. The fraction of monomers that are participating in multiple coordination to a single cation also decreases with increasing temperature (Figure 11c). Each monomer can be identified to participate in three different segment types based on the coordination number of the nearest cation; a linear segment ($CN^{O}_{BMIM^+} < 4$), a partially wrapping segment ($4 \leq CN^{O}_{BMIM^+} < 6$), or a ring segment ($CN^{O}_{BMIM^+} \geq 6$). At 300 K, about 40% of the monomers are in nonlinear segments, of which ∼12% are the ring segments. In contrast, about half of the monomers are not

DOI: 10.1021/acs.macromol.8b01002
Macromolecules 2018, 51, 5336−5345

coordinated to any cation at 600 K, and only 2% of the monomers (less than one monomer per PEO40 on average) are in ring segments.

The conformational transition between the ring and linear segments can be an important contributor to the temperature-dependent phase behavior. Unwrapping the ring segment from the cation would result in significant entropic gain and should be favored at high temperature. The release of coordinated ions with increasing temperature would ultimately lead into the experimentally observed LCST behavior. This hypothesized entropic mechanism of LCST is similar to the previously proposed ones[6,11] but does not rely on the short-ranged hydrogen-bonding interaction. In fact, a preliminary study of the concentrated mixture of PEO/$BMIM^+BF_4^-$ with SAPT-UA force field correctly captures the LCST despite the absence of explicit hydrogen atoms in the model.

The specific PEO/$BMIM^+BF_4^-$ interaction motifs depicted in Figure 10 are similar to what has been observed in PEO/Li-electrolyte systems,[33] which exhibit crown-ether-like coordination of Li^+ cations with multiple monomers of PEO.[34] In these related systems, both helical and cylindrical conformations of PEO are found to have high conductance because the Li^+ ions diffuse through the channel formed by the coordinating motifs.[35]

4.3. Dynamic Properties. The monomer mean-square displacements has possibly three regimes as a function of time. Figure 12a shows that the scaling of the MSD with time is consistent with $\sim t^{1/4}$ on time scales of tens of picoseconds, with $\sim t^{2/3}$ on time scales of a few nanoseconds, and with $\sim t^1$ on time scales of 100 ns. For a polymer in a homogeneous solvent these regimes could be interpreted as corresponding to confined, Zimm, and diffusive regimes. For the locally heterogeneous $BMIM^+BF_4^-$ solvent, interpretation of these regimes is less clear. The time take to reach diffusive behavior, i.e., ∼100 ns, is similar to the time scale for conformational relaxation, and the intermediate "Zimm" regime occurs on a length scale of several solvent diameters and may be interpreted as being due to hydrodynamic interactions.

We speculate that the confined regime corresponds to the time scale for the dissociation and exchange of the coordinating ions to the monomers. As shown in Figure 11d, the survival probability of the coordinating ions shows at least two distinct time scales at room temperature: a very rapid (<0.2 ns; see the inset) initial decay time and a much longer lifetime (tens of nanoseconds) of the coordinating ions. The shorter time scale is of the same order to the confined dynamics regime and corresponds to the short-lived loosely bound coordinating pair, which is dominated in the less coordinated linear segments. On the other hand, the highly coordinated cations can survive for tens of nanoseconds at room temperature, providing a partially rigid frame to the overall polymer structure. Also affected by the high viscosity of the IL solvent, the polymer is effectively confined at the locally heterogeneous environment at short time scale, and the monomers often diffuse by shifting between adjacent ions through coordination exchange. This is consistent with what we observe in movies of the polymer chain.

The scaling of the translational diffusion coefficient (D) of the polymer with M_w is shown in Figure 12b. $D \sim M_w^{\nu}$ with $\nu \approx 0.7$, but the statistical uncertainties are quite large. However, a plot of DR_g vs M_w is independent of molecular weight except for PEO9 (Figure S6), suggesting that the long time dynamics are consistent with the Zimm model.

5. SUMMARY AND CONCLUSIONS

We develop a first-principles, nonpolarizable united atom force field for PEO/$BMIM^+BF_4^-$ mixtures based on ab initio calculations. The effect of polarization is implicitly incorporated by fitting the PEO partial charge parameter in UA force field to reproduce the electrostatic cross-cohesive energy of PEO/$BMIM^+BF_4^-$ obtained from the fully polarizable all atomistic (AA) force field.[16] The resulting UA force field is in good agreement with the ab initio gas-phase PEO−cation dimer interaction and the AA condensed phase cohesive energy. The dihedral distribution of PEO chains has an important influence on the system density and chain conformations; and we therefore parametrize the intramolecular dihedral interaction parameters based on relaxed potential energy scans at the MP2 level of theory.[32]

The UA force field is computationally efficient and allows molecular dynamics simulations of several microseconds. Such long simulations are necessary because the conformational relaxation time of the polymer is several hundred nanoseconds, which is also the characteristic time for the polymer to reach the diffusive regime. The simulations are also made feasible because the force field is accurate (when compared to experiment) for the solvent dynamics. The model therefore combines the accuracy of fully polarizable models[16] while being *more* computationally efficient than empirical nonpolarizable force fields.[11,14,19] Multiple simulations, each microseconds long, are required to obtain the equilibrium properties of PEO (degree of polymerization 9−40) in $BMIM^+BF_4^-$.

We find that the chain size, characterized by the radius of gyration (R_g), scales with molecular weight as $R_g \sim M_w^{\nu}$ with $\nu \approx 0.56$, consistent with experiment.[13] The interesting feature is that segments of the polymer wrap around the cation, and the conformations are a combination of these "rings" combined with linear extended segments. The average size and its scaling with molecular weight do not provide a complete picture of the complex and interesting correlations between the polymer and the ionic liquid. It is also possible that these conformational motifs, which are similar to crown ether conformations for PEO in Li−electrolyte materials, could explain the entropic mechanism for the stabilization of the mixed phase at low temperatures. The monomer mean-square displacement shows three regimes which we interpret as confined, Zimm, and diffusive.

The simulations emphasize the importance of using accurate force fields and performing simulations of long enough duration. Previous simulation studies have reported different scaling behavior of PEO in $BMIM^+BF_4^-$. Mondal et al.[14] employed replica exchange molecular dynamics methods to study PEO conformations at room temperature. The swapping of conformations from different temperatures precluded the calculation of time correlation functions. However, if we require that one correlation time transpires before each replica exchange attempt, then their simulations were not long enough to adequately sample conformational space. Choi et al.[15] predicted collapsed chain scaling with a coarse-grained force field. The nature of the force field allowed an excessive wrapping of the polymer around the cation and thus collapsed the chain into solvent-separated globules. The scaling predictions at higher temperatures of 400 and 600 K with atomistic polarizable force fields[16] are consistent with the results of this work.

DOI: 10.1021/acs.macromol.8b01002
Macromolecules 2018, 51, 5336−5345

In conclusion, we present a computationally efficient force field for PEO in $BMIM^+BF_4^-$ which allows long enough simulations to adequately probe the conformations and dynamics of the polymer. This reveals interesting correlation effects caused by the strong interactions between the polymer and the strongly interacting ionic liquid solvent.

■ ASSOCIATED CONTENT

Supporting Information

The Supporting Information is available free of charge on the ACS Publications website at DOI: 10.1021/acs.macromol.8b01002.

Force field functional forms and optimized parameters; DFT-SAPT force field fits for homodimer UA models of PEO1 and PEO2; effect of the PEO charge parameter q_O of the SAPT-UA force field on the DFT-SAPT force field fits for homodimers of PEO1 and PEO2 and for the heterodimer of PEO2/$MMIM^+$ (PDF)

■ AUTHOR INFORMATION

Corresponding Author

*E-mail: yethiraj@chem.wisc.edu (A.Y.).

ORCID

Jesse G. McDaniel: 0000-0002-9211-1108

Qiang Cui: 0000-0001-6214-5211

Arun Yethiraj: 0000-0002-8579-449X

Notes

The authors declare no competing financial interest.

■ ACKNOWLEDGMENTS

This work was supported in part by US Department of Energy, Basic Energy Sciences, under Grant DE-SC0017877, the University of Wisconsin Materials Research Science and Engineering Center under Grant DMR-1121288, and the National Science Foundation under Grant CHE-1664906. Computational resources were provided by the Center for High Throughput Computing at the University of Wisconsin and the Extreme Science and Engineering Discovery Environment (XSEDE),[36] which is supported by National Science Foundation Grant ACI-1548562.

■ REFERENCES

(1) Rogers, R. D.; Seddon, K. R. Ionic Liquids-Solvents of the Future? *Science* **2003**, *302*, 792−793.

(2) Armand, M.; Endres, F.; MacFarlane, D. R.; Ohno, H.; Scrosati, B. Ionic-liquid Materials for the Electrochemical Challenges of the Future. *Nat. Mater.* **2009**, *8*, 621−629.

(3) Lodge, T. P. A Unique Platform for Materials Design. *Science* **2008**, *321*, 50−51.

(4) Ye, Y.-S.; Rick, J.; Hwang, B.-J. Ionic liquid polymer electrolytes. *J. Mater. Chem. A* **2013**, *1*, 2719−2743.

(5) Lee, H. N.; Lodge, T. P. Poly (n-butyl methacrylate) in Ionic Liquids with Tunable Lower Critical Solution Temperature (LCST). *J. Phys. Chem. B* **2011**, *115*, 1971−1977.

(6) Lee, H. N.; Newell, N.; Bai, Z. F.; Lodge, T. P. Unusual Lower Critical Solution Temperature Phase Behavior of Poly(ethylene oxide) in Ionic Liquids. *Macromolecules* **2012**, *45*, 3627−3633.

(7) Liu, F.; Lv, Y.; Liu, J.; Yan, Z.-c.; Zhang, B.; Zhang, J.; He, J.; Liu, C.-y. Crystallization and Rheology of Poly (ethylene oxide) in Imidazolium Ionic Liquids. *Macromolecules* **2016**, *49*, 6106−6115.

(8) Kelly, J. C.; Gupta, R.; Roberts, M. E. Responsive Electrolytes that Inhibit Electrochemical Energy Conversion at Elevated Temperatures. *J. Mater. Chem. A* **2015**, *3*, 4026−4034.

(9) Xiao, Z.; Larson, R. G.; Chen, Y.; Zhou, C.; Niu, Y.; Li, G. Unusual Phase Separation and Rheological Behavior of Poly(ethylene oxide)/Ionic Liquid Mixtures with Specific Interactions. *Soft Matter* **2016**, *12*, 7613−7623.

(10) Asai, H.; Fujii, K.; Nishi, K.; Sakai, T.; Ohara, K.; Umebayashi, Y.; Shibayama, M. Solvation Structure of Poly(ethylene glycol) in Ionic Liquids Studied by High-energy X-ray Diffraction and Molecular Dynamics Simulations. *Macromolecules* **2013**, *46*, 2369−2375.

(11) Choi, E.; Yethiraj, A. Entropic Mechanism for the Lower Critical Solution Temperature of Poly(ethylene oxide) in a Room Temperature Ionic Liquid. *ACS Macro Lett.* **2015**, *4*, 799−803.

(12) Triolo, A.; Russina, O.; Keiderling, U.; Kohlbrecher, J. Morphology of Poly(ethylene oxide) Dissolved in a Room Temperature Ionic Liquid: A Small Angle Neutron Scattering Study. *J. Phys. Chem. B* **2006**, *110*, 1513−1515.

(13) Kharel, A.; Lodge, T. P. Coil Dimensions of Poly(ethylene oxide) in an Ionic Liquid by Small-Angle Neutron Scattering. *Macromolecules* **2017**, *50*, 8739−8744.

(14) Mondal, J.; Choi, E.; Yethiraj, A. Atomistic Simulations of Poly(ethylene oxide) in Water and an Ionic Liquid at Room Temperature. *Macromolecules* **2014**, *47*, 438−446.

(15) Choi, E.; Mondal, J.; Yethiraj, A. Coarse-Grained Models for Aqueous Polyethylene Glycol Solutions. *J. Phys. Chem. B* **2014**, *118*, 323−329.

(16) McDaniel, J. G.; Choi, E.; Son, C. Y.; Schmidt, J. R.; Yethiraj, A. Conformational and Dynamic Properties of Poly(ethylene oxide) in an Ionic Liquid: Development and Implementation of a First-Principles Force Field. *J. Phys. Chem. B* **2016**, *120*, 231−243.

(17) Mcdaniel, J. G.; Choi, E.; Son, C. Y.; Schmidt, J. R.; Yethiraj, A. Ab Initio Force Fields for Imidazolium-Based Ionic Liquids. *J. Phys. Chem. B* **2016**, *120*, 7024−7036.

(18) Salanne, M. Simulations of Room Temperature Ionic Liquids: From Polarizable to Coarse-Grained Force Fields. *Phys. Chem. Chem. Phys.* **2015**, *17*, 14270−14279.

(19) Son, C. Y.; McDaniel, J. G.; Schmidt, J. R.; Cui, Q.; Yethiraj, A. First-Principles United Atom Force Field for the Ionic Liquid $BMIM^+BF_4^-$: An Alternative to Charge Scaling. *J. Phys. Chem. B* **2016**, *120*, 3560−3568.

(20) Pronk, S.; Páll, S.; Schulz, R.; Larsson, P.; Bjelkmar, P.; Apostolov, R.; Shirts, M. R.; Smith, J. C.; Kasson, P. M.; van der Spoel, D.; Hess, B.; Lindahl, E. GROMACS 4.5: A High-Throughput and Highly Parallel Open Source Molecular Simulation Toolkit. *Bioinformatics* **2013**, *29*, 845−854.

(21) Darden, T.; York, D.; Pedersen, L. Particle Mesh Ewald: An Nlog(N) Method for Ewald Sums in Large Systems. *J. Chem. Phys.* **1993**, *98*, 10089−10092.

(22) Essmann, U.; Perera, L.; Berkowitz, M. L.; Darden, T.; Lee, H.; Pedersen, L. G. A Smooth Particle Mesh Ewald Method. *J. Chem. Phys.* **1995**, *103*, 8577−8593.

(23) Nosé, S. A Molecular Dynamics Method for Simulations in the Canonical Ensemble. *Mol. Phys.* **1984**, *52*, 255−268.

(24) Hoover, W. Canonical Dynamics: Equilibrium Phase-Space Distributions. *Phys. Rev. A: At., Mol., Opt. Phys.* **1985**, *31*, 1695−1697.

(25) Berendsen, H. J. C.; Postma, J. P. M.; van Gunsteren, W. F.; DiNola, A.; Haak, J. R. Molecular Dynamics with Coupling to an External Bath. *J. Chem. Phys.* **1984**, *81*, 3684−3690.

(26) Parrinello, M.; Rahman, A. Polymorphic Transitions in Single Crystals: A New Molecular Dynamics Method. *J. Appl. Phys.* **1981**, *52*, 7182−7190.

(27) Hesselmann, A.; Jansen, G.; Schütz, M. Density-Functional Theory-Symmetry-Adapted Intermolecular Perturbation Theory with Density Fitting: A New Efficient Method to Study Intermolecular Interaction Energies. *J. Chem. Phys.* **2005**, *122*, 014103−014119.

(28) Misquitta, A. J.; Jeziorski, B.; Szalewicz, K. Dispersion Energy from Density-Functional Theory Description of Monomers. *Phys. Rev. Lett.* **2003**, *91*, 33201−33204.

(29) Misquitta, A. J.; Szalewicz, K. Symmetry-Adapted Perturbation-Theory Calculations of Intermolecular Forces Employing Density-

DOI: 10.1021/acs.macromol.8b01002
Macromolecules 2018, 51, 5336−5345

Functional Description of Monomers. *J. Chem. Phys.* **2005**, *122*, 214109−214127.
(30) McDaniel, J. G.; Schmidt, J. R. Physically-Motivated Force Fields From Symmetry-Adapted Perturbation Theory. *J. Phys. Chem. A* **2013**, *117*, 2053−2066.
(31) Briggs, J. M.; Matsui, T.; Jorgensen, W. L. Monte Carlo simulations of liquid alkyl ethers with the OPLS potential functions. *J. Comput. Chem.* **1990**, *11*, 958−971.
(32) Anderson, P. M.; Wilson, M. R. Developing a Force Field for Simulation of Poly (ethylene oxide) Based Upon ab initio Calculations of 1, 2-Dimethoxyethane. *Mol. Phys.* **2005**, *103*, 89−97.
(33) Jankowski, P.; Dranka, M.; Wieczorek, W.; Johansson, P. TFSI and TDI Anions: Probes for Solvate Ionic Liquid and Disproportionation-Based Lithium Battery Electrolytes. *J. Phys. Chem. Lett.* **2017**, *8*, 3678−3682.
(34) MacGlashan, G.; Andreev, Y.; Bruce, P. Structure of the Polymer Electrolyte Poly(ethylene oxide)$_6$: LiAsF$_6$. *Nature* **1999**, *398*, 792−794.
(35) Gitelman, L.; Averbuch, A.; Nathan, M.; Schuss, Z.; Golodnitsky, D. Stochastic Model of Lithium Ion Conduction in Poly(ethylene oxide). *J. Appl. Phys.* **2010**, *107*, 064318.
(36) Towns, J.; Cockerill, T.; Dahan, M.; Foster, I.; Gaither, K.; Grimshaw, A.; Hazlewood, V.; Lathrop, S.; Lifka, D.; Peterson, G. D.; Roskies, R.; Scott, J. R.; Wilkens-Diehr, N. XSEDE: Accelerating Scientific Discovery. *Comput. Sci. Eng.* **2014**, *16*, 62−74.

DOI: 10.1021/acs.macromol.8b01002
Macromolecules 2018, 51, 5336−5345